

# Unsupervised Two-Stage Anomaly Detection

Yunfei Liu      Chaoqun Zhuang      Feng Lu\*

State Key Laboratory of Virtual Reality Technology and Systems,  
School of Computer Science and Engineering, Beihang University, Beijing, China

{lyunfei, zhuangchaoqun, lufeng}@buaa.edu.cn

## Abstract

*Anomaly detection from a single image is challenging since anomaly data is always rare and can be with highly unpredictable types. With only anomaly-free data available, most existing methods train an AutoEncoder to reconstruct the input image and find the difference between the input and output to identify the anomalous region. However, such methods face a potential problem – a coarse reconstruction generates extra image differences while a high-fidelity one may draw in the anomaly (Fig.1). In this paper, we solve this contradiction by proposing a two-stage approach, which generates high-fidelity yet anomaly-free reconstructions. Our Unsupervised Two-stage Anomaly Detection (UTAD) relies on two technical components, namely the Impression Extractor (IE-Net) and the Expert-Net. The IE-Net and Expert-Net accomplish the two-stage anomaly-free image reconstruction task while they also generate intuitive intermediate results, making the whole UTAD interpretable. Extensive experiments show that our method outperforms state-of-the-arts on four anomaly detection datasets with different types of real-world objects and textures.*

## 1. Introduction

Most objects or textures in nature have certain shapes and properties, especially human-made ones. Anomaly detection identifies rare items, events, or observations that raise suspicions by differing significantly from the majority [6]. It will translate to many computer vision tasks, such as detect defective product parts [10], segment lesions in retinopathy images [34], and locate intruders in surveillance [33], etc. Anomaly detection is challenging since most deep learning-based methods require balanced positive data and negative data for training. However, abnormal data is always limited, and hard or even cannot be obtained in terms of their amount and types.

To tackle the lack of abnormal data, many methods as-

sume the novel things that occurred on the *category* or *image-level* are anomalies. They detect if a new input is out-of-distribution when compared with the training data. These methods can be referred to as one-class-classification or outlier detection [4, 32, 41, 46]. However, this setting is not suitable for anomaly detection, which pays more attention on the images within the same category. In this case, anomalies often exist in small areas in the object or image (e.g., crack on the surface, missing small parts, etc.).

Recently, many approaches tackle this challenging problem with AutoEncoders [8, 12, 13, 20] and GAN based methods [2, 3, 44], which assume the network cannot reconstruct the unseen regions, then find the input and its difference with the output to identify the anomaly. Although such methods are able to distinguish novel classes from old ones (e.g., find the novel class in MNIST [27] or CIFAR-10 [26], etc.), these methods face a potential contradiction. As shown in Fig.1 (a), coarse reconstructions generate extra image difference, which interrupts the anomaly detection. To reconstruct more high-fidelity details, many methods[3, 40] equip with more complex architectures or more trainable parameters. However, the output may draw the anomaly in and loses the anomaly-related difference.

In this paper, we tackle this contradiction with two steps to ensure anomaly-free and high-fidelity, respectively. More specifically, we introduce a mediate state, namely impression  $m$ , which is the anomaly-free reconstruction of the input. Then we design a two stage framework to generate both anomaly-free and high-fidelity reconstruction for anomaly detection. As illustrated in Fig. 1 (c), our idea is to generate the anomaly-free and high-fidelity  $\hat{x}$  through two stages. Consequently, we introduce the Unsupervised Two-stage Anomaly Detection (UTAD) framework, which contains two key components: the Impression Extractor (IE-Net) and the Expert-Net. The IE-Net is used for the first-stage reconstruction, which generates the anomaly-free  $m$  for the given input  $x$  (Sec. 3.1). The Expert-Net then restores details on  $m$  for the high-fidelity  $\hat{x}$  (Sec. 3.2). Finally, we use Perceptual Measurement ( $PM$ ) to better detect anomaly-related differences among the input  $x$ , impression  $m$  and reconstructed  $\hat{x}$

\*Corresponding author.

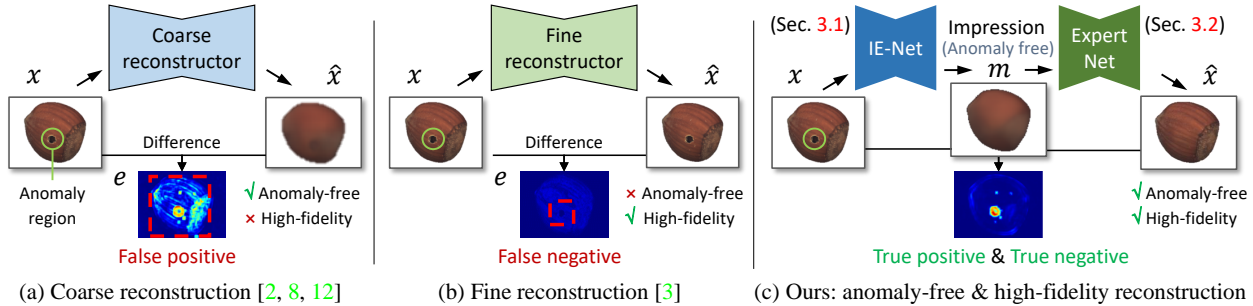


Figure 1. Comparisons of different anomaly detection methods. Many one-stage methods reconstruct the structure of the input but without details (A) [2, 8, 12] or high-fidelity reconstruction yet draw in anomaly regions (B) [3]. (c) We tackle the contradiction by extracting the anomaly-free structure ( $m$ ) and adding high-fidelity details in two stages.

(Sec. 3.3).

In summary, our main contributions are:

- We propose a novel Unsupervised Two-stage Anomaly Detection (UTAD) framework that enables both anomaly-free and high-fidelity reconstruction for anomaly detection from a single image. The method requires no anomaly sample for training.
- We propose the new concept of anomaly-free reconstruction (namely impression) for anomaly detection. We design an IE-Net and Expert-Net to extract and utilize impression for anomaly-free and high-fidelity reconstructions, respectively.
- The proposed UTAD framework outperforms state-of-the-arts on four anomaly detection datasets with different types of real-world objects and textures.

## 2. Related Works

### 2.1. Unsupervised anomaly detection

Many AutoEncoder-based methods are proposed for unsupervised anomaly detection. Carrera *et al.* [13] train an AutoEncoder and make it over-fit on the anomalous-free images, then use the magnitude of reconstruction loss (*i.e.*, MSE loss) on test images to determine anomalous regions. Based on this, Bergmann *et al.* [12] propose to replace per-pixel MSE loss with structure similarity loss [49]. Baur *et al.* [8] propose to use a variational auto-encoder (VAE) instead of the auto-encoder. There are also many GAN [39] based methods for anomaly detection. AnoGAN [44] is the first to use a generator for unsupervised anomaly detection on retinopathy images. Inspired by AnoGAN, GANomaly [2] adds an encoder for mapping images to latent space, and greatly decreases the inference time. Fast-AnoGAN [43] trains a WGAN [5] and an additional encoder with two stages to boost the performance. Berg *et al.* [9] propose to combine progressive growing GAN [24] and ClusterGAN [31] together to reconstruct high-resolution images for anomaly detection. Skip-GANomaly [3] replaces the auto-encoder with

U-net [40] and further gets better reconstructions. However, such methods face a potential problem of whether making a coarse reconstruction or a high-fidelity one – the former generates extra image differences while the latter may draw the anomaly in and lose the anomaly-related difference.

Based on the uncertainty learning, Bergmann *et al.* [11] propose Uniformed Students, which use the teacher-students for unsupervised anomaly detection. However, the learning process is kind of verbose and with limited interpretation. Venkataramanan *et al.* [48] propose to use an attention mechanism, and use the activated feature for anomaly detection. There are also other methods that use additional supervision [52] or memory bank [20] for anomaly detection.

### 2.2. One class classification

One class classification (*i.e.*, outlier detection) is concerned with distinguishing out-of-detection samples relative to the training set. SVDD [46] tries to map all the normal training data into predefined kernel space and takes the sample that outside the learned distribution as anomaly. Andrews *et al.* [4] use the different layer features from the pre-trained VGG network and model the anomaly-free images with a  $v$ -SVM. There are many methods that equip this idea with patched distribution clustering [32] or extend it to a semi-supervised scenario [41]. There is a major difference between the one-class classification and anomaly detection since one class classification detects images from a different category, while anomaly detection aims to detect and locate the difference between images that are from the same class.

### 2.3. Unsupervised Representation learning

Learning a good representation of an image is a long-standing problem of computer vision. One branch of research suggests training the encoder by learning with a *pre-text task* (*e.g.*, predicting relative patch location [17], solving a jigsaw puzzle [35], coloring images [51], counting objects [36], and predicting rotations [19]). Another branch of research suggests extracting the unique information of the sample so that the sample can be distinguished easily for the downstream tasks. Based on this assumption, many mutual

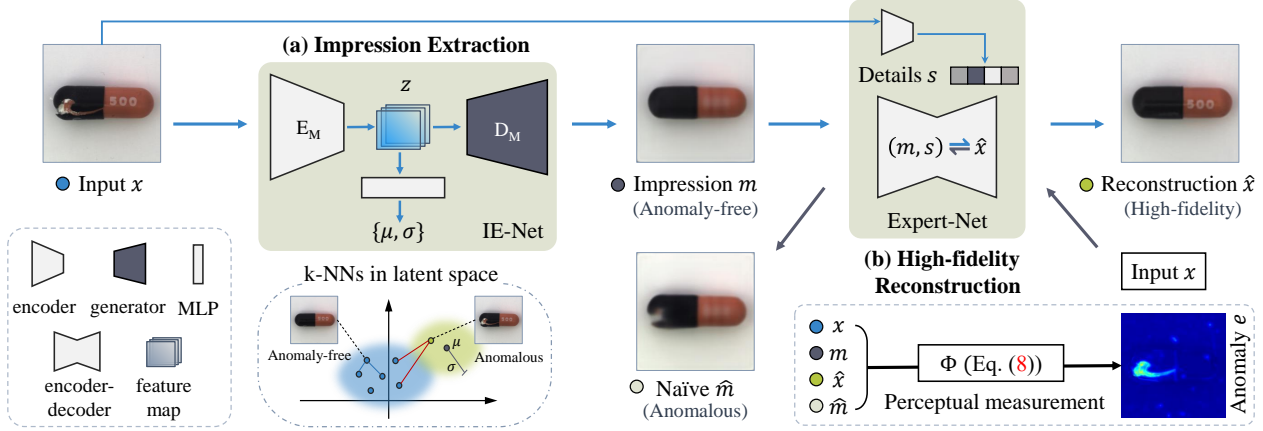


Figure 2. Overview of the proposed method. Our framework mainly contains two components: *IE-Net* and *Expert-Net*. (a) *IE-Net* tries to generate the anomaly-free reconstruction (*i.e.*, impression  $m$ ). (b) The *Expert-Net* aims to learn an invertible mapping to manipulate the high-fidelity details between impression  $m$  and input  $x$ . Finally, the anomaly map  $e$  is calculated through *Perceptual Measurement*  $\Phi$  by leveraging the difference among  $x$ ,  $\hat{x}$ ,  $m$ , and  $\hat{m}$ .

information-based methods are proposed, like f-GAN [37], info-GAN [14], info-NCE [47], and AMDIM [7], *etc.* In this paper, we are inspired by the mutual information and propose to learn the distinctive and anomaly-free features for the anomaly detection task.

### 3. Unsupervised Two-stage Anomaly Detection

Here we introduce the proposed Unsupervised Two-stage Anomaly Detection (UTAD) for unsupervised anomaly detection. Given a training set  $\mathcal{D} = \{x_1, x_2, \dots, x_N\}$  of anomaly-free images, our goal is to learn two different networks that serve two stages for anomaly detection without any anomalous samples. As shown in Fig. 2, UTAD is constructed by

- *Impression Extractor Network* (*IE-Net*) extracts the anomaly-free impression  $m$  on the input  $x$ .
- *Expert-Net* is an invertible mapping, which generates details on  $m$  to produce the high-fidelity reconstruction  $\hat{x}$ . Meanwhile, for a better performance and interpretation, it also produces an intermediate naïve impression  $\hat{m}$  by mimicking the appearance of the output of *IE-Net*.

#### 3.1. *IE-Net* for anomaly-free reconstruction

*IE-Net* aims to reconstruct the anomaly-free impression  $m$  for anomaly detection. The output of *IE-Net* is used as the input of *Expert Net*, which will be introduced in Sec. 3.2. **Training phase.** The *IE-Net* is trained on the anomaly-free dataset. The architecture of *IE-Net* is illustrated in Fig. 3. *IE-Net* is constructed by an encoder  $E_M$ , a discriminator  $T$  and a decoder  $D_M$ . These modules are jointly optimized by minimizing objective Eq. (6).

**Inference phase.** When *IE-Net* is trained on the anomaly-free dataset, its encoder  $E_M$  and  $D_M$  are used for generating

anomaly-free impression  $m$  for the input image, which may contain anomalous regions.

Since it is not trivial to control the reconstruction ability for anomaly detection, as illustrated in Fig. 1, we propose to extract the input image with anomaly-free impression  $m$  on the basis of mutual information theory. Specifically, we equip *IE-Net* with mutual information mainly because 1) mutual information is used to describe the distinctive features of the input image [47] and 2) only anomaly-free samples are used for training. Therefore, the anomaly-free and distinctive features are suitable for reconstructing the impression.

As illustrated in Fig. 3, the encoder  $E_M$  aims to extract the distinctive feature  $z$  of the image  $x$  by maximizing the mutual information  $I(\mathcal{D}, Z)$ , where  $z \in Z$ ,  $Z$  is the set of latent codes.  $I(\mathcal{D}, Z)$  is defined as follow

$$I(\mathcal{D}, Z) = \int \int p(z|x)p(x) \log \frac{p(z|x)}{p(z)} dx dz, \quad (1)$$

where  $p(x)$  is the distribution of  $\mathcal{D}$ . Following the assumptions in VAE [25], the distribution  $p(z)$  is required to follow the Gaussian distribution  $q(z)$ , which is implemented by Kullback-Leibler (KL) divergence

$$KL(p(z) \parallel q(z)) = \int p(z) \log \frac{p(z)}{q(z)} dz. \quad (2)$$

As with maximizing the mutual information, the loss function of the encoder  $E_M(x)$  becomes

$$\mathcal{L}_M^e = -I(\mathcal{D}, Z) + \lambda KL(p(z) \parallel q(z)), \quad (3)$$

where  $\lambda$  is the hyper-parameter for balancing these two terms in the objective function. To optimize Eq. (1), we follow f-GAN [37] and convert the maximizing process of mutual



$\hat{x}$ ,  $\hat{m}$  and intermediate  $\hat{s}$  are constrained to  $x$ ,  $m$ ,  $s$  through L1 loss, respectively.

### 3.3. Perceptual measurement for anomaly detection

Traditional methods [3, 43] identify the anomaly by using the pixel-wise difference (e.g., L1, MSE). To effectively detect the anomaly regions, we find that using perceptual measurement (PM) among images on anomaly detection can achieve better performance. Perceptual distance has also been successfully applied to other tasks such as image synthesis and style transfer [23]. When inference, given an unknown image  $x$ , the corresponding  $\{m, \hat{x}, \hat{m}\}$  are estimated through UTAD. The anomaly map  $e$  of the unknown image is calculated through perceptual distance:

$$e = \Phi(x, \hat{x}, m, \hat{m}) = \sum_l \lambda_l^e (\phi_l(x, \hat{x}) + \phi_l(m, \hat{m}) + \phi_l(x, m)), \quad (8)$$

where  $\phi(\cdot)$  is the feature distance (i.e., perceptual distance, which measures the L1 distance of features in a pre-trained VGG-19 network).

Based on the anomaly error map  $e$ , the anomaly region segmentation  $y$  is calculated below

$$y(i, j) = \begin{cases} 1, & \text{if } e(i, j) > \alpha; \\ 0, & \text{otherwise,} \end{cases} \quad (9)$$

where  $i, j$  are pixel index of error map  $e$  and  $\alpha$  is threshold for anomaly segmentation.

## 4. Experiments

To demonstrate the effectiveness of the proposed UTAD, extensive evaluation and rigorous analysis of ablation studies on a number of datasets are performed.

### 4.1. Experimental setup

**Benchmark datasets.** We evaluate our UTAD on the MVTEC AD [10] with 15 different objects and textures for anomaly detection. Furthermore, MNIST [27], Fashion MNIST [50], and CIFAR-10 [26] are also used for anomaly detection.

**Baseline methods.** We compare UTAD with OCGAN [38], AnoGAN [44], AVID [42], AE<sub>L2</sub> [12], AE<sub>SSIM</sub> [12], LSA [1], and AD-VAE [29] with their publicly official code. Since the official project of UnSt [11] and  $\gamma$ -VAE [16] are not publicly available, we use their third-party implementations<sup>12</sup>, respectively. We have also compared our method with the unsupervised version of CAVGA [48].

**Implementation details.** The detailed implementation of the proposed method is organized as follow:

<sup>1</sup><https://github.com/denguir/student-teacher-anomaly-detection>

<sup>2</sup><https://github.com/dbbbbm/energy-projection-anomaly>

- **IE-Net.** The encoder  $E_M$  is constructed by 4 inception blocks [45]. Each of them is followed by a max-pooling layer for down-sampling the feature map. The decoder  $D_M$  contains 4 inception blocks with a  $2\times$  nearest up-sample layer, then followed by a  $1\times 1$  convolutional layer with sigmoid activation for the reconstruction of the impression. The MLP is constructed by a stack of three fully connected layers. The discriminator  $T$  is constructed by a 4-layer MLP with a sigmoid activation layer at the endpoint.
- **Expert-Net.** Based on MUNIT [23], the encoders ( $E_X^A, E_X^B$ ) of the Expert-Net contains 4 convolutional blocks and 2 residual blocks. The decoder is constructed by 2 residual blocks with AdaIN as normalization layer, then followed 4 convolutional blocks with upsamples to reconstruct the image. The *detail extractor*  $E_S$  contains 3 convolutional layers and follows an adaptive average pooling layer.
- **PM.** To effectively involve different features for anomaly detection, we select the layers ‘conv1\_2’, ‘conv2\_2’, and ‘conv3\_4’ in the VGG-19 network and set  $\lambda_1^e = \lambda_2^e = \lambda_3^e = 1$  in our experiments. We empirically set  $\alpha = 0.5$  for anomaly segmentation.

### 4.2. Comparisons to SOTAs

We evaluate our method on 15 category-specific dataset with high-resolution images (i.e., MVTEC AD [10]) and three low-resolution datasets (MNIST [27], Fashion MNIST [50], and CIFAR-10 [26]).

**MVTEC AD dataset.** For all experiments on MVTEC AD, images are re-scaled to  $w = h = 256$  for training and inference. We train the IE-Net on anomaly-free images for 200 epochs with batch size 4. We use SGD with initial learning rate  $10^{-3}$  and momentum 0.9. For Expert-Net, we use Adam with learning rate  $10^{-3}$ . Fig. 5 illustrates the visual comparisons among different methods. Our method localizes more accurate and fine-grained anomalous regions than the compared methods. Since the CAVGA is not publicly available, we directly use the results from their supplement materials. As illustrated in Fig. 6, our method makes anomaly-free and high-fidelity reconstructions when compared to the two typical one-state methods [12, 3]. Table 1 shows the quantitative comparison over Intersection over Union (IoU) and Area under ROC curve (AuROC). Our method outperforms the state-of-the-art method (CAVGA) in mean IoU by 6%.

**MNIST, Fashion MNIST and CIFAR-10.** On the MNIST, Fashion-MNIST, and CIFAR-10 datasets, we follow the same settings as in [15] (i.e., training/testing uses a single class as normal and the rest of the classes as anomalous. Each image is zoomed to  $w = h = 64$  for training and inference. Because the resolution and input size of these

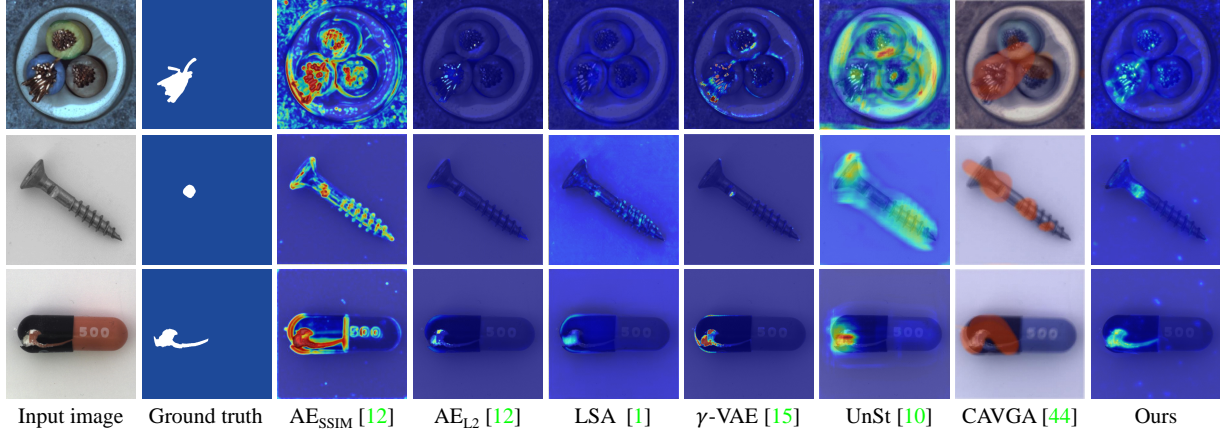


Figure 5. Qualitative comparisons among different methods on MVTec AD dataset.

Table 1. Quantitative comparison of anomaly detection in category-specific IoU, mean IoU ( $\overline{\text{IoU}}$ ) and mean AuROC ( $\overline{\text{AuROC}}$ ) on the MVTec AD dataset. The best results are highlighted with bold font, and the second bests are underlined.

Category	AnoGAN [44]	AVID [42]	AE <sub>L2</sub> [12]	AE <sub>SSIM</sub> [12]	LSA [1]	AD-VAE [29]	$\gamma$ -VAE [16]	UnSt [11]	CAVGA [48]	Ours
Bottle	0.05	0.28	0.22	0.15	0.27	0.27	0.27	0.28	<u>0.34</u>	<b>0.37</b>
Cable	0.01	0.27	0.05	0.01	0.36	0.18	0.26	0.11	<b>0.38</b>	<b>0.38</b>
Capsule	0.04	0.21	0.11	0.09	0.22	0.11	0.24	0.24	<u>0.31</u>	<b>0.41</b>
Carpet	0.34	0.25	0.38	0.69	0.76	0.10	<b>0.79</b>	0.50	0.73	<b>0.79</b>
Grid	0.04	0.51	0.83	<u>0.88</u>	0.20	0.02	0.36	0.19	0.38	<b>0.89</b>
Hazelnut	0.02	0.54	0.41	0.00	0.41	0.44	<u>0.63</u>	0.36	0.51	<b>0.65</b>
Leather	0.34	0.32	0.67	0.34	0.77	0.24	0.41	0.44	<b>0.79</b>	<b>0.79</b>
Metal Nut	0.00	0.05	0.26	0.01	0.38	<b>0.49</b>	0.22	0.31	0.45	0.47
Pill	0.17	0.11	0.25	0.07	0.18	0.18	<u>0.48</u>	0.23	0.40	<b>0.49</b>
Screw	0.01	0.22	0.34	0.03	0.38	0.17	0.38	0.17	<b>0.48</b>	<u>0.44</u>
Tile	0.08	0.09	0.23	0.04	0.32	0.23	0.38	0.22	<u>0.38</u>	<b>0.40</b>
Toothbrush	0.07	0.43	0.51	0.08	0.48	0.14	0.37	0.21	<b>0.57</b>	<u>0.53</u>
Transistor	0.08	0.22	0.22	0.01	0.21	0.30	<u>0.44</u>	0.15	0.35	<b>0.47</b>
Wood	0.14	0.14	0.29	0.36	0.41	0.14	0.45	0.16	<b>0.59</b>	<b>0.59</b>
Zipper	0.01	<u>0.25</u>	0.13	0.10	0.14	0.06	0.17	0.08	0.16	<b>0.30</b>
$\overline{\text{IoU}}$	0.09	0.26	0.33	0.19	0.37	0.20	0.39	0.24	<u>0.47</u>	<b>0.53</b>
$\overline{\text{AuROC}}$	0.74	0.78	0.82	0.87	0.79	0.86	0.86	0.87	<u>0.89</u>	<b>0.90</b>

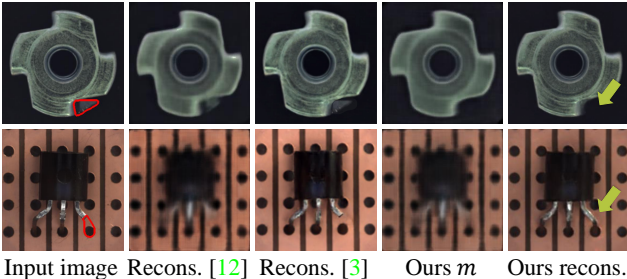


Figure 6. Our method generates **anomaly-free** impression  $m$  and its **high-fidelity** reconstruction. The anomaly areas are highlighted in the input images with red contours.

three datasets are lower than those in MVTec AD dataset, we adjust the architecture of IE-Net and Expert-Net to fit these cases. Specifically, we reduce the number of inception blocks to 3 in IE-Net. Meanwhile, we set the number of residual blocks to 1 in Expert-Net. Table 2 shows the quantitative comparison results. We find the ablation studies verify different components of our framework. Our proposed outperforms the other methods for many settings.

### 4.3. Interpretation and analysis

#### Interpretation of UTAD.

Interpretation can be performed with two folds: illustration of intermediate results of UTAD and visualization of feature distributions. As illustrated in Fig. 7, it is clear that

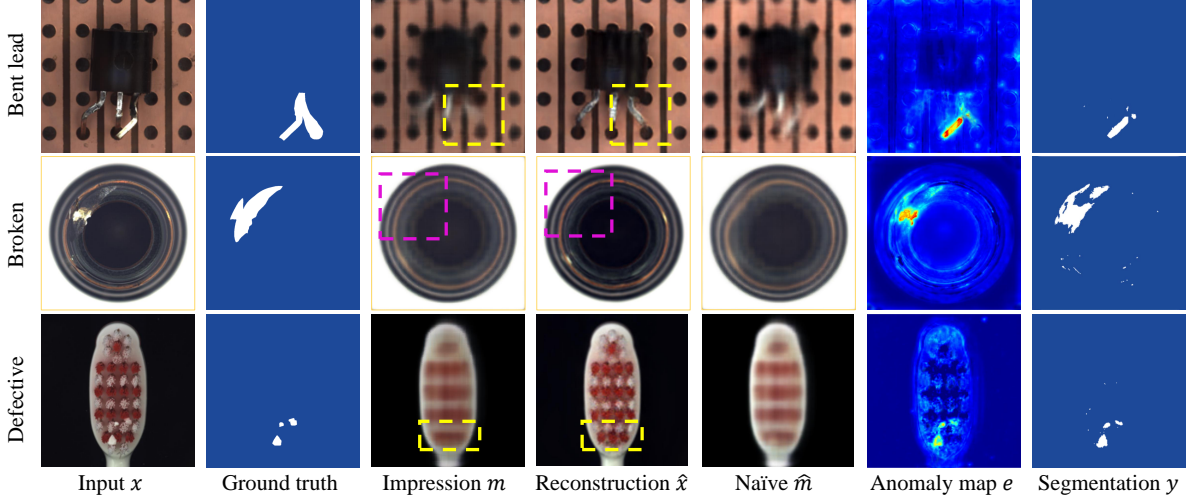


Figure 7. Interpretation of the intermediate results in UTAD. As illustrated in dashed boxes, the impression  $m$  is robust to anomalous regions, while the naïve impression  $\hat{m}$  is affected by the anomalous regions.

Table 2. Quantitative comparison of different methods and ablation study on MNIST ( $D_M$ ), Fashion MNIST ( $D_F$ ) and CIFAR-10 ( $D_C$ ) datasets. Here we use mean AuROC as the evaluation metric.

Existing method	$D_M$	$D_F$	$D_C$
OCGAN [38]	0.975	0.895	0.657
AnoGAN [44]	0.937	0.824	0.612
SkipGA [3]	0.941	0.807	0.731
LSA [1]	0.975	0.641	0.876
AE <sub>L2</sub> [12]	0.983	0.747	0.790
CapsNet [28]	0.871	0.679	0.531
UnSt [11]	0.993	-	0.803
CAVGA [48]	0.986	0.885	0.737

Ablation	$L_{info}$	EN	Guide	$\hat{m}$	$D_M$	$D_F$	$D_C$
Baseline					0.979	0.743	0.787
Ours	✓				0.981	0.751	0.803
Ours		✓			0.989	0.885	0.861
Ours	✓	✓			0.988	0.890	0.872
Ours		✓	✓		0.993	0.891	0.876
Ours	✓	✓	✓		0.992	0.894	0.881
Ours	✓	✓	✓	✓	<b>0.994</b>	<b>0.899</b>	<b>0.884</b>

the impression  $m$  automatically fixes the anomaly region. Based on the impression, the Expert-Net reconstructs the exact details of the anomaly-free image  $\hat{x}$ . Meanwhile, the naïve impression version  $\hat{m}$  often contains the anomaly area with the total image become blurry. Next, the anomaly region  $e$  is calculated by a pixel-wise scoring as Eq. (8), in which pixels in the anomaly region have higher scores than that in the anomaly-free region. Fig. 8 shows the learned distributions of anomaly-free images and anomalous images. It can be found that the anomaly image and anomalous image are with different mean and variance. Furthermore, based

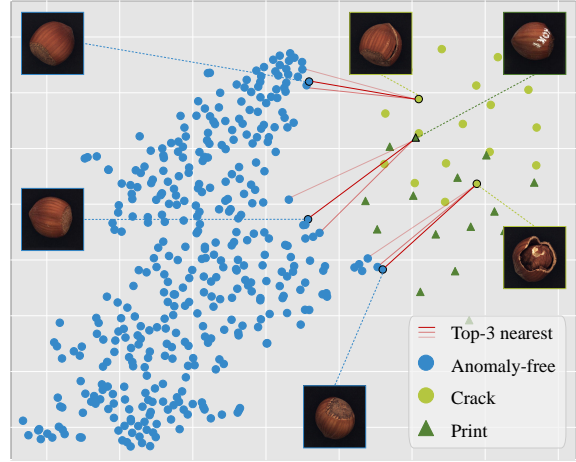


Figure 8. Analysis of the learned features in IE-Net. Feature distributions of anomaly-free images (blue) and anomalous images (green) are illustrated via t-SNE [30].

on the mutual information, one can be found the k-Nearest anomaly-free images when the anomalous image is given. For instance, the cracked hazelnut share a similar pose with the matched anomaly-free one at the top of Fig. 8. Here two types of anomalous images are given (*i.e.*, crack and print).

#### Ablation study.

To evaluate how different parts of UTAD contribute to the final performance on the two tasks, we conduct rigorous ablation studies by removing or replacing a subset of models. Details of different baselines are described as follows:

- *Without maximizing mutual information* (Without  $L_{info}$ ). To illustrate the contribution of the mutual information learning for impression extraction, we remove this part and re-train the remaining model.
- *Effectiveness of Expert-Net* (Without EN). To examine

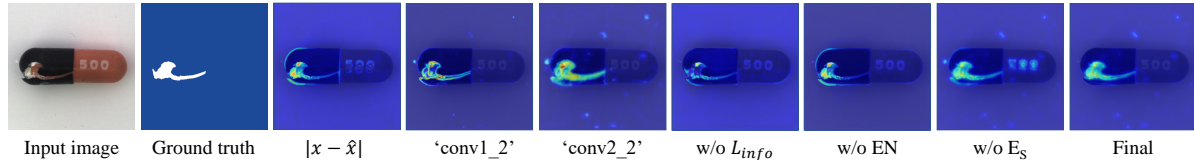


Figure 9. Qualitative comparison of different combinations of our method on anomaly detection.

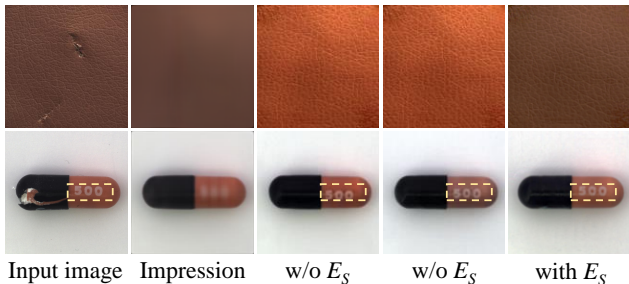


Figure 10. Illustration of the effectiveness of detail guidance module  $E_S$ . Two results are provided without  $E_S$  (Column 3-4). With  $E_S$ , some inconsistencies in details *e.g.*, color-shift (top row) and misplaced text (*i.e.*, ‘500’, dashed box in bottom row) are tackled.

the effectiveness of Expert-Net in anomaly detection, we remove Expert-Net totally and the anomaly error map  $e$  is calculated by  $e = \sum_l (\phi_l(x, m))$ .

- *Detail Guidance module (Without  $E_S$ )*. To examine the contribution of the guidance from detailed information, we remove the  $E_S$  and feed the input of AdaIN in the decoder of Expert-Net with random weights of Gaussian distributions (*i.e.*,  $N(0, 1)$ ).

The ablation studies are mainly performed on 10 categories on the MNIST, Fashion MNIST, and CIFAR-10 datasets. The mean AuROC of each dataset is shown in Table 2. Since for UnSt [11], one teacher net and 5 student nets are trained, it performs exceptionally well on these small datasets. However, on average, our method still outperforms all evaluated approaches. Furthermore, the visual comparison is provided in the 6th - 8th column in Fig 9. Without  $L_{info}$ , the anomaly region cannot be corrected detected. Without  $EN$ , misaligned edges occur in anomaly detection. Anomaly-free regions on the capsule are mistakenly detected as anomaly when the  $E_S$  is removed (the detail code  $s$  is generated with random numbers). More visual results are provided in Fig. 10.

#### Different measurements for anomaly detection.

A variety of measurements for anomaly detection has been tested on MVTEC AD dataset. Numerical comparisons of different measurements on 4 objects are listed in Table 3. The combination of ‘conv1\_2’, ‘conv2\_2’ and ‘conv3.4’ (*i.e.*,  $PM$ ) gets the best performance on different objects. We find the difference of features from ‘conv2\_2’ gets secondary performance. The performance is decreased in ‘conv3.4’ since the resolution is too small. As illustrated in Fig. 9, It can be clearly found that the pixel-level or low-level differences like

$|x - \hat{x}|$  and ‘conv1\_2’ are sensible on the local difference, but often misled by misalignment. Meanwhile, the high-level difference (*i.e.*, ‘conv2\_2’) gets relative correct regions. The result of  $PM$  gets the best visual quality.

Table 3. Ablation study. Performance comparison among differences between input and intermediate results and different choices of layers in VGG-19 on part of MVTEC AD dataset.

Measurement	Bottle	Cable	Capsule	Hazelnut
$ x - \hat{x} $	0.23	0.17	0.33	0.39
$ x - \hat{m} $	0.29	0.20	0.21	0.47
$ m - \hat{m} $	0.15	0.06	0.15	0.41
‘conv1_2’	0.30	0.11	0.33	0.39
‘conv2_2’	0.33	0.31	0.35	0.54
‘conv3.4’	0.24	0.20	0.31	0.49
$PM$	<b>0.37</b>	<b>0.38</b>	<b>0.41</b>	<b>0.65</b>

#### Effect of the model capacity.

Finally, we investigate the relationship between the model capacity and anomaly detection performance. Numerical results on MVTEC AD Hazelnut are reported in Table 4. We find that more learnable parameters, which result in better reconstruction ability of an AutoEncoder (AE) [12], do not help the anomaly detection. This confirms our observation in Fig. 1. On the other hand, benefiting from the proposed two-stage reconstruction scheme, our method outperforms UnSt [11] with a similar number of parameters.

Table 4. Effect of parameters’ number in training.

Methods	AE-64	AE-128	AE-256	UnSt [11]	Ours
# Param (M)	2.98	11.89	47.47	14.28	16.77
IoU ( $\uparrow$ )	0.301	0.188	0.197	0.363	<b>0.649</b>
AuROC ( $\uparrow$ )	0.896	0.954	0.945	0.937	<b>0.976</b>

## 5. Conclusion

In this paper, we propose a novel method (*i.e.*, the Unsupervised Two-stage Anomaly Detection) for unsupervised anomaly detection in natural images. In particular, we propose to utilize a two-stage framework (*i.e.*, IE-Net, Expert-Net) for anomaly detection. The IE-Net and Expert-Net are used to generate high-fidelity and anomaly-free reconstructions of the input. UTAD generates rich and intuitive intermediate results, make the framework interpretable. Extensive experiments demonstrate state-of-the-art performance on different datasets, which contain different types of real-world objects and textures.

## References

- [1] Davide Abati, Angelo Porrello, Simone Calderara, and Rita Cucchiara. Latent space autoregression for novelty detection. In *CVPR*, 2019. 5, 6, 7
- [2] Samet Akcay, Amir Atapour-Abarghouei, and Toby P Breckon. Ganomaly: Semi-supervised anomaly detection via adversarial training. In *ACCV*. Springer, 2018. 1, 2
- [3] Samet Akçay, Amir Atapour-Abarghouei, and Toby P Breckon. Skip-ganomaly: Skip connected and adversarially trained encoder-decoder anomaly detection. In *IJCNN*. IEEE, 2019. 1, 2, 5, 7
- [4] Jerone Andrews, Thomas Tanay, Edward J Morton, and Lewis D Griffin. Transfer representation-learning for anomaly detection. In *ICML*. JMLR, 2016. 1, 2
- [5] Martin Arjovsky, Soumith Chintala, and Léon Bottou. Wasserstein gan. *arXiv preprint arXiv:1701.07875*, 2017. 2
- [6] Zimek Arthur and Schubert Erich. Outlier detection. *Encyclopedia of Database Systems*, 2017. 1
- [7] Philip Bachman, R Devon Hjelm, and William Buchwalter. Learning representations by maximizing mutual information across views. In *NeurIPS*, 2019. 3
- [8] Christoph Baur, Benedikt Wiestler, Shadi Albarqouni, and Nassir Navab. Deep autoencoding models for unsupervised anomaly segmentation in brain mr images. In *International MICCAI Brainlesion Workshop*. Springer, 2018. 1, 2
- [9] Amanda Berg, Jörgen Ahlberg, and Michael Felsberg. Unsupervised learning of anomaly detection from contaminated image data using simultaneous encoder training. *arXiv preprint arXiv:1905.11034*, 2019. 2
- [10] Paul Bergmann, Michael Fauser, David Sattlegger, and Carsten Steger. Mvtec ad—a comprehensive real-world dataset for unsupervised anomaly detection. In *CVPR*, 2019. 1, 5
- [11] Paul Bergmann, Michael Fauser, David Sattlegger, and Carsten Steger. Uninformed students: Student-teacher anomaly detection with discriminative latent embeddings. In *CVPR*, 2020. 2, 5, 6, 7, 8
- [12] Paul Bergmann, Sindy Löwe, Michael Fauser, David Sattlegger, and Carsten Steger. Improving unsupervised defect segmentation by applying structural similarity to autoencoders. *arXiv preprint arXiv:1807.02011*, 2018. 1, 2, 5, 6, 7, 8
- [13] Diego Carrera, Fabio Manganini, Giacomo Boracchi, and Ettore Lanzarone. Defect detection in sem images of nanofibrous materials. *IEEE Transactions on Industrial Informatics*, 2016. 1, 2
- [14] Xi Chen, Yan Duan, Rein Houthoofd, John Schulman, Ilya Sutskever, and Pieter Abbeel. Infogan: Interpretable representation learning by information maximizing generative adversarial nets. In *NeurIPS*, 2016. 3
- [15] Lucas Deecke, Robert Vandermeulen, Lukas Ruff, Stephan Mandt, and Marius Kloft. Image anomaly detection with generative adversarial networks. In *ECML*. Springer, 2018. 5
- [16] David Dehaene, Oriel Frigo, Sébastien Combexelle, and Pierre Eline. Iterative energy-based projection on a normal data manifold for anomaly localization. In *CVPR*, 2020. 5, 6
- [17] Carl Doersch, Abhinav Gupta, and Alexei A Efros. Unsupervised visual representation learning by context prediction. In *ICCV*, 2015. 2
- [18] Yixiao Ge, Dapeng Chen, and Hongsheng Li. Mutual mean-teaching: Pseudo label refinery for unsupervised domain adaptation on person re-identification. In *ICLR*, 2020. 4
- [19] Spyros Gidaris, Praveer Singh, and Nikos Komodakis. Unsupervised representation learning by predicting image rotations. In *ICLR*, 2018. 2
- [20] Dong Gong, Lingqiao Liu, Vuong Le, Budhaditya Saha, Moussa Reda Mansour, Svetha Venkatesh, and Anton van den Hengel. Memorizing normality to detect anomaly: Memory-augmented deep autoencoder for unsupervised anomaly detection. In *ICCV*, 2019. 1, 2
- [21] Kaiming He, Haoqi Fan, Yuxin Wu, Saining Xie, and Ross Girshick. Momentum contrast for unsupervised visual representation learning. In *CVPR*, 2020. 4
- [22] Xun Huang and Serge Belongie. Arbitrary style transfer in real-time with adaptive instance normalization. In *CVPR*, 2017. 4
- [23] Xun Huang, Ming-Yu Liu, Serge Belongie, and Jan Kautz. Multimodal unsupervised image-to-image translation. In *ECCV*, 2018. 4, 5
- [24] Tero Karras, Timo Aila, Samuli Laine, and Jaakko Lehtinen. Progressive growing of gans for improved quality, stability, and variation. *arXiv preprint arXiv:1710.10196*, 2017. 2
- [25] Diederik P Kingma and Max Welling. Auto-encoding variational bayes. *arXiv preprint arXiv:1312.6114*, 2013. 3
- [26] Alex Krizhevsky, Geoffrey Hinton, et al. Learning multiple layers of features from tiny images. 2009. 1, 5
- [27] Yann LeCun, Léon Bottou, Yoshua Bengio, and Patrick Haffner. Gradient-based learning applied to document recognition. *Proceedings of the IEEE*, 1998. 1, 5
- [28] Xiaoyan Li, Iluju Kiringa, Tet Yeap, Xiaodan Zhu, and Yifeng Li. Exploring deep anomaly detection methods based on capsule net. In *CCAI*. Springer, 2020. 7
- [29] Wenqian Liu, Runze Li, Meng Zheng, Srikrishna Karanam, Ziyang Wu, Bir Bhanu, Richard J Radke, and Octavia Camps. Towards visually explaining variational autoencoders. In *CVPR*, 2020. 5, 6
- [30] Laurens van der Maaten and Geoffrey Hinton. Visualizing data using t-sne. *Journal of machine learning research*, 2008. 7
- [31] Sudipto Mukherjee, Himanshu Asnani, Eugene Lin, and Sreeram Kannan. Clustergan: Latent space clustering in generative adversarial networks. In *AAAI*, 2019. 2
- [32] Paolo Napoletano, Flavio Piccoli, and Raimondo Schettini. Anomaly detection in nanofibrous materials by cnn-based self-similarity. *Sensors*, 2018. 1, 2
- [33] Phuc Nguyen, Ting Liu, Gautam Prasad, and Bohyung Han. Weakly supervised action localization by sparse temporal pooling network. In *CVPR*, 2018. 1
- [34] Yuhao Niu, Lin Gu, Feng Lu, Feifan Lv, Zongji Wang, Imari Sato, Zijian Zhang, Yangyan Xiao, Xunzhang Dai, and Tingting Cheng. Pathological evidence exploration in deep retinal image diagnosis. In *AAAI*, 2019. 1
- [35] Mehdi Noroozi and Paolo Favaro. Unsupervised learning of visual representations by solving jigsaw puzzles. In *ECCV*. Springer, 2016. 2

- [36] Mehdi Noroozi, Hamed Pirsiavash, and Paolo Favaro. Representation learning by learning to count. In *ICCV*, 2017. [2](#)
- [37] Sebastian Nowozin, Botond Cseke, and Ryota Tomioka. f-gan: Training generative neural samplers using variational divergence minimization. In *NeurIPS*, 2016. [3](#)
- [38] Pramuditha Perera, Ramesh Nallapati, and Bing Xiang. Oc-gan: One-class novelty detection using gans with constrained latent representations. In *CVPR*, 2019. [5](#), [7](#)
- [39] Alec Radford, Luke Metz, and Soumith Chintala. Unsupervised representation learning with deep convolutional generative adversarial networks. In *ICLR*, 2016. [2](#)
- [40] Olaf Ronneberger, Philipp Fischer, and Thomas Brox. U-net: Convolutional networks for biomedical image segmentation. In *MICCI*. Springer, 2015. [1](#), [2](#)
- [41] Lukas Ruff, Robert A Vandermeulen, Nico Görnitz, Alexander Binder, Emmanuel Müller, Klaus-Robert Müller, and Marius Kloft. Deep semi-supervised anomaly detection. In *ICLR*, 2020. [1](#), [2](#)
- [42] Mohammad Sabokrou, Masoud Pourreza, Mohsen Fayyaz, Rahim Entezari, Mahmood Fathy, Jürgen Gall, and Ehsan Adeli. Avid: Adversarial visual irregularity detection. In *ACCV*. Springer, 2018. [5](#), [6](#)
- [43] Thomas Schlegl, Philipp Seeböck, Sebastian M Waldstein, Georg Langs, and Ursula Schmidt-Erfurth. f-anogan: Fast unsupervised anomaly detection with generative adversarial networks. *Medical image analysis*, 2019. [2](#), [5](#)
- [44] Thomas Schlegl, Philipp Seeböck, Sebastian M Waldstein, Ursula Schmidt-Erfurth, and Georg Langs. Unsupervised anomaly detection with generative adversarial networks to guide marker discovery. In *International conference on information processing in medical imaging*. Springer, 2017. [1](#), [2](#), [5](#), [6](#), [7](#)
- [45] Christian Szegedy, Wei Liu, Yangqing Jia, Pierre Sermanet, Scott Reed, Dragomir Anguelov, Dumitru Erhan, Vincent Vanhoucke, and Andrew Rabinovich. Going deeper with convolutions. In *CVPR*, 2015. [5](#)
- [46] David MJ Tax and Robert PW Duin. Support vector data description. *Machine learning*, 2004. [1](#), [2](#)
- [47] Michael Tschannen, Josip Djolonga, Paul K Rubenstein, Sylvain Gelly, and Mario Lucic. On mutual information maximization for representation learning. In *ICLR*, 2020. [3](#)
- [48] Shashanka Venkataramanan, Kuan-Chuan Peng, Rajat Vikram Singh, and Abhijit Mahalanobis. Attention guided anomaly detection and localization in images. In *ECCV*, 2020. [2](#), [5](#), [6](#), [7](#)
- [49] Zhou Wang, Alan C Bovik, Hamid R Sheikh, and Eero P Simoncelli. Image quality assessment: from error visibility to structural similarity. *IEEE transactions on image processing*, 2004. [2](#)
- [50] Han Xiao, Kashif Rasul, and Roland Vollgraf. Fashion-mnist: a novel image dataset for benchmarking machine learning algorithms. *arXiv preprint arXiv:1708.07747*, 2017. [5](#)
- [51] Richard Zhang, Phillip Isola, and Alexei A Efros. Colorful image colorization. In *ECCV*. Springer, 2016. [2](#)
- [52] Kang Zhou, Yuting Xiao, Jianlong Yang, Jun Cheng, Wen Liu, Weixin Luo, Zaiwang Gu, Jiang Liu, and Shenghua. Gao.

Encoding structure-texture relation with p-net for anomaly detection in retinal images. In *ECCV*, 2020. [2](#)